



# Automatic-switching-based teleoperation framework for mobile manipulator with asymmetrical mapping and force feedback<sup>☆,☆☆</sup>

Wenwen Li <sup>a,c</sup>, Fanghao Huang <sup>a,b,c,\*</sup>, Zihao Chen <sup>c</sup>, Zheng Chen <sup>a,c</sup>

<sup>a</sup> State Key Laboratory of Fluid Power and Mechatronic Systems, Zhejiang University, Hangzhou, 310027, People's Republic of China

<sup>b</sup> Fujian Key Laboratory of Green Intelligent Drive and Transmission for Mobile Machinery, Huaqiao University, Xiamen, 361021, People's Republic of China

<sup>c</sup> Ocean College, Zhejiang University, Zhoushan, 316021, People's Republic of China



## ARTICLE INFO

### Keywords:

Mobile manipulator  
Teleoperation  
Heterogeneity  
Automatic switching  
Asymmetrical mapping  
Force feedback

## ABSTRACT

Teleoperation technology has become a feasible solution for the mobile manipulator to carry out complex tasks in remote environments, with its advantages of mobility and manipulability. However, due to the high redundancy of the mobile manipulator, its application in the field of teleoperation inevitably suffers from the problem of heterogeneity. This paper proposed an automatic-switching-based teleoperation framework with asymmetrical mapping and force feedback. Namely, special coefficients are designed to automatically switch the motion states of the remote robot, so that the traditional manual-based switching strategy can be replaced. Based on these coefficients, the hybrid asymmetrical mapping including the position–velocity and position–position modes can be achieved, as well as the force feedback considering the switching between the remote mobile platform and the manipulator, and thereby accomplishing the automatic switching during the teleoperation of the mobile manipulator. The comparative experiments and user study were carried out on the teleoperation platform. The experimental results show that this proposed teleoperation framework can reduce the time needed to complete the tasks and decrease the decision-making pressure of the operator, thus demonstrating the feasibility of the proposed framework.

## 1. Introduction

The mobile manipulator (MM) is primarily composed of a mobile platform and a manipulator [1], which enables the end-effector to achieve the desired motion through the coordinated movement of the mobile platform and manipulator [2,3]. The MM fuses the mobility of a wheeled platform and the manipulability of a fixed manipulator [4], making it widely applicable in fields [5] such as manufacturing, construction, agriculture, and military industries. However, autonomous robots cannot be well applied in some special fields, such as aerospace [6], deep-sea exploration [7,8], nuclear radiation [9, 10], and other fields that are challenging and hazardous for humans to reach, and the complex tasks involved in these fields make MM hard to work independently due to constraints imposed by the industries. Therefore, the human–robot–environment interacted teleoperation technology may be a feasible solution to achieve higher performance of the MM [11]. A typical teleoperation system mainly consists

of the operator, the local device, the communication channel, the remote robot and the environment [12].

Inevitably, due to the high redundancy of the MM, the application of teleoperation technology in it may suffer from the problem of master–slave heterogeneity (MSH). This is generally defined as the difference in mechanical structures, sizes and number of joints between the local and remote robots, which is almost inevitable in the practical application of teleoperation system. Currently, the majority of research on teleoperation focuses on time-delay-based stability [13,14] and teleoperation transparency [15,16]. However, when a remote task is directly executed, the characteristics of MSH will impel the operator to make extra effort in mapping the movements between the local and remote robots [17], which will add extra workload to the operator and worsen the operation effect, especially for MM with an integrated vehicle-manipulator. Therefore, it is necessary to conduct teleoperation heterogeneous planning for MM, and the more important

<sup>☆</sup> This work is supported by National Natural Science Foundation of China (No. 52301404, No. 52075476), Zhejiang Provincial Natural Science Foundation of China (No. LR23E050001), China Postdoctoral Science Foundation, China (No. 2023M743001), Zhejiang Provincial Postdoctoral Research Excellent Funding Project (No. ZJ2023050), Open Foundation of Fujian Key Laboratory of Green Intelligent Drive and Transmission for Mobile Machinery (No. GIDT-202302) and Fundamental Research Funds for the Central Universities, China (No. 226-2023-00029, No. 2022FZZX01-06).

<sup>☆☆</sup> This paper was recommended for publication by Associate Editor Takeshi Hatanaka.

\* Corresponding author at: State Key Laboratory of Fluid Power and Mechatronic Systems, Zhejiang University, Hangzhou, 310027, People's Republic of China.

E-mail address: [huangfanghao@zju.edu.cn](mailto:huangfanghao@zju.edu.cn) (F. Huang).

issues among them include vehicle-manipulator motion coordination, unmatched workspace and force feedback matching.

As for vehicle-manipulator motion coordination, a common approach is to control the mobile platform and the manipulator separately using a joystick and a haptic device, respectively. However, it should be noted that this operation mode will exert great physical and mental burden on the operator and increase the system's cost. For this reason, many researchers focus on finding a solution to use a single device to operate both the mobile platform and the manipulator, which is called operation allocation in this paper. At present, operation allocation is mainly based on switching control, which includes manual [18] and automatic [19–21] switching. Although manual switching is often applied in practical applications due to its simplicity, there also exist the problems such as high operating pressure and low operating efficiency. Therefore, automatic switching is proposed to solve the problem of manual switching, while trying to improve the performance of the task by implementing remote operation with less mental load. In [20], it is proposed to decouple the motion control of MM and divide the workspace of the local robot to realize the automatic switching. In [22], it is proposed to set virtual mass-spring-damping forces between the end-effector (EE) of the remote manipulator and the camera, so the operator only needs to control the motion of the EE, while the vehicle with the camera will follow naturally. The automatic switching method of setting virtual devices to assist navigation is proposed in [23]. However, most of the current automatic switching methods are discontinuous, so the remote system will have an unstable switching state, or some switching methods rely on the local state excessively, which still brings pressure to the operator.

Regarding the unmatched workspace, different mapping algorithms are considered to cover the remote workspace as much as possible. For fixed-base manipulators, existing studies generally utilize scaling position-position mapping [24], while for mobile robots, the same position is mapped to the velocity command (position-velocity) [25]. Combining these two mapping modes, a hybrid position-velocity and position-position mapping strategy for the teleoperation of a mobile robot is proposed in [26], and the switching is carried out by pressing the buttons. Meanwhile, in [27], it is proposed to divide the local workspace to switch between these two mapping modes. However, few works have jointly addressed the problem of discontinuous automatic switching and asymmetrical mapping.

Apart from the above problems, force feedback is another important issue that may affect the operator's experience [28]. In a general teleoperation system, due to the limited visual fields of the camera carried by the remote robot, dangerous effects such as collisions with obstacles may regularly occur. Meanwhile, remote operation with auxiliary force feedback is a common way in teleoperation, which further enhances the operator's telepresence. However, matching the force feedback according to remote tasks is also challenging [29]. Usually, it only feeds back the operation force between the remote manipulator and the environment [30], or the virtual guidance force of the mobile robot obtained according to the environmental information [31–33]. For instance, a variable feedback gain method based on the velocity of approaching obstacles is proposed in [32]. In [33], it is proposed to use the artificial potential field (APF) method to establish the virtual guidance force of the mobile robot. However, the authors have found few works that synthetically analyze the force feedback of both the mobile platform and the manipulator.

Above all, most of the existing works mainly address a single problem in the heterogeneous planning for the teleoperation of MM, such as manual [18] and automatic [20,22,23] switching methods for vehicle-manipulator motion coordination, asymmetric mapping for unmatched workspace (such as scale mapping [34], incremental mapping, position-velocity mapping [24,25], etc.), and incomplete force feedback [31–33]. There has been little prior work on this topic of the integrated issues.

Therefore, in this paper, a continuous automatic-switching-based teleoperation framework, including asymmetric mapping and force feedback matching, is developed for the MSH system of MM to deal with the problem of heavy workload and low operation efficiency caused by MSH. Noting that many studies have been conducted on the time-delay of teleoperation, this paper mainly focuses on improving the operation performance by utilizing heterogeneous planning of the master-slave workspace and force feedback mapping, thereby reducing operator's workload and enhancing overall efficiency. Therefore, the impact of time-delay on system stability is not considered for the time being. The main contributions are summarized as follows:

1. A hybrid asymmetrical mapping framework based on automatic switching is designed, which aims to automatically switch the motion states of the remote robot. Namely, the coefficients that can smoothly change with the local command and the remote environment are designed as the motion switcher of the remote robot. Based on these coefficients, a hybrid asymmetrical mapping including position-velocity and position-position modes is proposed, so that the local limited reachable workspace can cover the infinite workspace of the remote robot.

2. Based on automatic switching, an integrated force feedback mapping algorithm is designed, which is matched with the remote tasks. As a result, compared to visual feedback alone, the operator can better sense the changes in the remote environment with the assistance of automatic force feedback.

3. Comparative experiments and user study were carried out on the teleoperation system, which is consisted of the local haptic device Phantom Omni and the remote KUKA-Youbot. The experiment results have evaluated and verified that this automatic-switching-based teleoperation framework can effectively reduce the execution time of the same task and decrease the decision-making pressure on the operator compared with the traditional manual-based framework.

The remainder of this paper is organized as follows. The preliminary of the kinematic model and the problem formulation is addressed in Section 2. An integrated teleoperation framework for MM is introduced in Section 3. In Section 4, the semi-physical simulation experiment is carried out at first, and the experimental setup and results are provided in Section 5. The conclusions are summarized in Section 6.

## 2. Preliminaries

### 2.1. Modeling of the teleoperation system

The commercial haptic device Phantom Omni [27,28,34] with 6 degrees of freedom (DOFs) is selected as the local robot. The end position  $P_m$  of the local device can be obtained using the modified Denavit-Hartenberg(D-H) method, with D-H parameter table shown in Table 1, while  $Q_m$  can be obtained as (1), where  $\theta_{mi}, i = 1, 2, 3$  is the  $i$ th joint angle of the local robot,  $r_m$  is the projection of the distance between the end position and the coordinate origin of the robot on the  $xy$  plane, and  $h_m$  is the height of the end position, as shown in Fig. 1.

$$\begin{cases} r_m = l_{m1} \cos \theta_{m2} + l_{m2} \sin (\theta_{m2} + \theta_{m3}) \\ h_m = l_{m1} \sin \theta_{m2} - l_{m2} \cos (\theta_{m2} + \theta_{m3}) \end{cases} \quad (1)$$

The KUKA-Youbot [35,36], a typical MM, is a four mecanum wheeled mobile robot surmounted by a 5 DOFs manipulator with a 2 DOFs gripper. Similarly, its forward kinematics solution is shown in Fig. 1, and can be obtained as (2).

$$\begin{cases} r_s = l_{s2} \sin \theta_{s2} + l_{s3} \sin \theta_{s23} + l_{s4} \sin \theta_{s234} \\ h_s = l_{s1} + l_{s2} \cos \theta_{s2} + l_{s3} \cos \theta_{s23} + l_{s4} \cos \theta_{s234} \end{cases} \quad (2)$$

where,  $\theta_{s23} = \theta_{s2} + \theta_{s3}$ ,  $\theta_{s234} = \theta_{s2} + \theta_{s3} + \theta_{s4}$ .

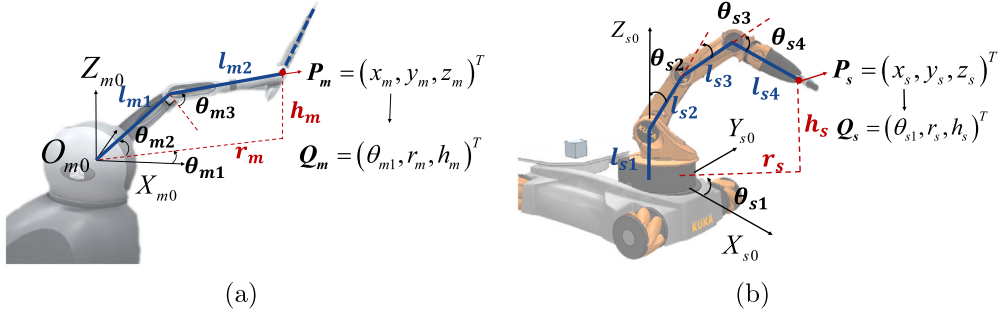


**Fig. 1.** Forward kinematics of local robot and remote manipulator: (a) Forward kinematics of local robot (corresponding to Eq. (1)), (b) Forward kinematics of remote manipulator (corresponding to Eq. (2)).

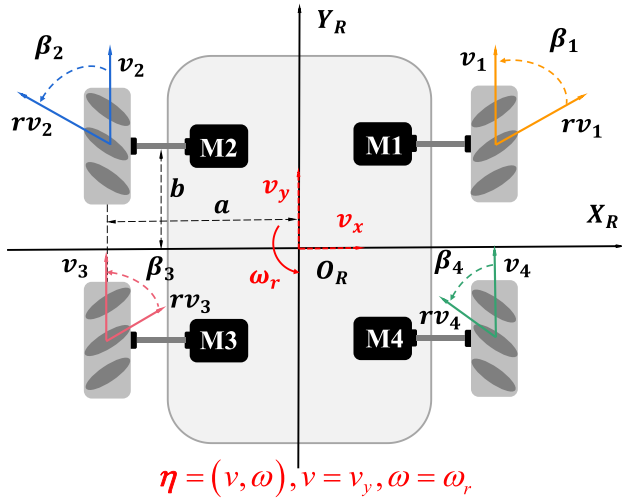


**Fig. 2.** Kinematics solution of the mobile platform.

**Table 1**  
The D-H parameters of the local robot.

$i$	$\alpha_i$	$a_i$	$d_i$	$\theta_i$
1	0	0	0	$q_1$
2	$\pi/2$	0	0	$q_2$
3	0	$l_1$	0	$\pi/2 + q_3$
4	$-\pi/2$	0	$l_2$	$q_4$
5	$\pi/2$	0	0	$-\pi/2 + q_5$
6	$-\pi/2$	0	0	$\pi + q_6$

For the mobile platform of the remote robot, its kinematics solution is shown in Fig. 2, and can be obtained as (3).

$$\begin{bmatrix} \omega_1 \\ \omega_2 \\ \omega_3 \\ \omega_4 \end{bmatrix} = \frac{1}{R} \begin{bmatrix} -1 & 1 & (a+b) \\ 1 & 1 & -(a+b) \\ -1 & 1 & -(a+b) \\ 1 & 1 & (a+b) \end{bmatrix} \begin{bmatrix} v_x \\ v_y \\ \omega_r \end{bmatrix}, \quad (3)$$

where \$R\$ is the wheel radius, \$v\_x\$ and \$v\_y\$ are the velocities of the mobile platform in \$x\$ and \$y\$ directions, respectively, \$\omega\_r\$ is the angular velocity of the mobile platform rotation, and \$\omega\_i (i = 1, 2, 3, 4)\$ is the angular velocity of the wheel rotation. Then the velocity vector of the mobile platform is defined as \$\eta = (v, \omega)\$, \$v = v\_y\$, \$\omega = \omega\_r\$.

Next, the inverse kinematics of the remote manipulator is solved without considering the end pose. In order to simplify the inverse

kinematics solution process, geometric conditions of the manipulator configuration are added according to the different situation, as shown in Fig. 3. The distance between the end position \$O\_4\$ and the origin of the second joint coordinate \$O\_1\$ is set as \$l\_x\$, and \$\theta\_{s5}\$ is always set to 0.

When \$l\_x \in (l\_{s3} + \sqrt{l\_{s4}^2 - l\_{s2}^2}, l\_{s2} + l\_{s3} + l\_{s4})\$, the parallel condition is constructed (as shown in Fig. 3(a)), that is, \$l\_x\$ is parallel to \$l\_{s3}\$, so that the angle values of each joint can be obtained as (4).

$$\begin{cases} \theta_{s3} = \pm \arccos \left( \frac{l_{s3}^2 + l_{x1}^2 - l_{x2}^2}{2l_{s3}l_{x1}} \right) \\ \theta_{s4} = \pm \arccos \left( \frac{l_{s3}^2 + l_{x2}^2 - l_{x1}^2}{2l_{s3}l_{x2}} \right) \\ \theta_{s2} = a \tan 2(h_s - l_{s1}, r_s) - \theta_{s3} \end{cases} \quad (4)$$

While when \$l\_x < l\_{s3} + \sqrt{l\_{s4}^2 - l\_{s2}^2}\$, the parallel condition cannot be constructed and the vertical condition (as shown in Fig. 3(b)) is adopted, that is, \$l\_{s2}\$ is vertical to \$l\_{s3}\$, so that the angle values of each joint can be obtained as (5).

$$\begin{cases} \theta_{s4} = \pi - \arccos \left( \frac{l_{s4}^2 + l_{x1}^2 - l_x^2}{2l_{s4}l_{x1}} \right) \\ \theta_{s2} = a \tan 2(h_s - l_{s1}, r_s) \pm \arccos \left( \frac{l_x^2 + l_{x2}^2 - l_{s4}^2}{2l_{x2}l_x} \right) \pm \arccos \left( \frac{l_{s2}^2 + l_{x2}^2 - l_{s3}^2}{2l_{s2}l_{x2}} \right) \\ \theta_{s3} = \frac{\pi}{2} \end{cases} \quad (5)$$

## 2.2. Problem formulation

Different from the traditional teleoperation framework for MM, the framework proposed in this paper is based on automatic switching to achieve asymmetrical mapping and force feedback mapping design.

In order to obtain the mapping relationship from the local position command \$P\_m\$ to the remote velocity \$\eta\$ and position reference \$P\_s\$, and match the force feedback \$F\_e\$ with the remote tasks, the designed teleoperation framework should achieve the following requirements:

- Heterogeneous matching performance: \$P\_m\$ should be simultaneously mapped to \$\eta\$ and \$P\_s\$ through the hybrid position-velocity and position-position asymmetrical mapping, which is to make full use of the remote workspace, while the switching between the two mapping modes should be automatic and smooth.
- Force feedback performance: The force \$F\_e\$, which is converted from the remote environment and fed back to the operator, should be matched with the remote tasks and bounded.
- Experiment evaluation: Compared with traditional button-based teleoperation methods, the quantitative indicator \$P\_o\$, which represents the workload of the operator, should be designed to carry out the user study to verify the superiority of the proposed

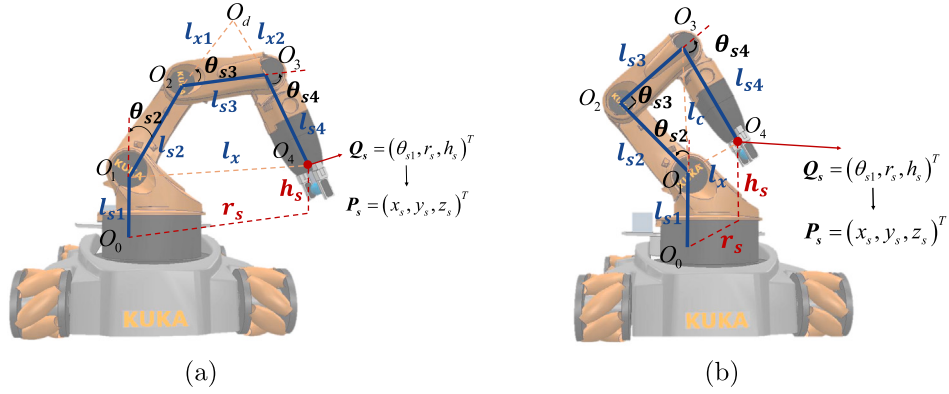


**Fig. 3.** Inverse kinematics of the remote manipulator under two conditions: (a) Parallel condition ( $l_x$  is parallel to  $l_{s3}$ ), i.e., the ligature between  $O_2$  and  $O_3$  is parallel to the ligature between  $O_1$  and  $O_4$ , (b) Vertical condition ( $l_{s2}$  is vertical to  $l_{s3}$ ), i.e., the ligature between  $O_1$  and  $O_2$  is vertical to the ligature between  $O_2$  and  $O_3$ .

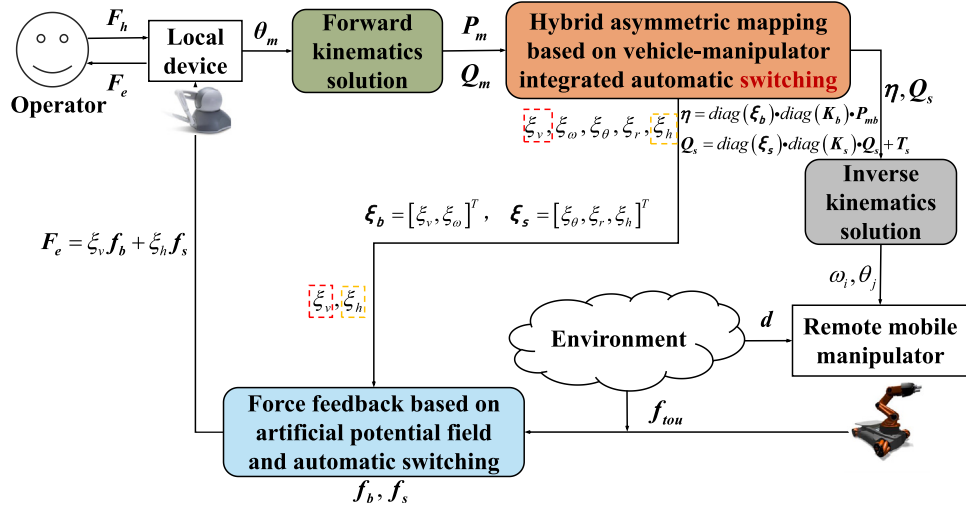


**Fig. 4.** The overall automatic-switching-based teleoperation framework for the mobile manipulator.

framework.  $P_o$  of the proposed framework should be lower than that of the traditional methods.

### 3. Automatic-switching-based teleoperation framework

#### 3.1. Overall framework

The overall automatic-switching-based teleoperation framework for MM is shown in Fig. 4. Firstly, the operator manipulates the local device to generate the joint information  $\theta_m$ . Then, the position command  $P_m$  and  $Q_m$  of the local device can be obtained by forward kinematics solution, therefore, through the hybrid asymmetrical mapping based on automatic switching, the position signals are mapped to the velocity  $\eta$  of the mobile platform and the end position  $Q_s$  of the remote manipulator, respectively. Then  $Q_s$  and  $\eta$  are sent to the remote side, while the angular velocity  $\omega_i$  of the mobile platform wheels and the joint angles  $\theta_j$  of the manipulator are obtained through the inverse kinematics solution. Meanwhile, through force feedback based on the APF and automatic switching, which considers both the force feedback  $f_b$  of the mobile platform and the force feedback  $f_s$  of the remote manipulator, the distance information is mapped to the force  $F_e$ . Among them, the automatic switching coefficients ( $\xi_v, \xi_\omega, \xi_\theta, \xi_r, \xi_h$ ) are designed and applied to the hybrid mapping and force feedback to form the automatic-switching-based teleoperation framework. Therefore, the motion state of the remote robot can be switched automatically, without requiring the operator to pay attention to the switching process.

#### 3.2. Automatic-switching-based hybrid asymmetrical mapping

The asymmetrical mapping relationship of the local and remote robots in this system is shown in Fig. 5, which maps the 3D position ( $\mathbf{P}_m = (x_m, y_m, z_m)^T$ ) of the local robot into the 2 DOF reference of the mobile platform ( $\boldsymbol{\eta} = (v, \omega)^T$ ) and the 3 DOF reference of the manipulator ( $\mathbf{Q}_s = (x_s, y_s, z_s)^T$ ).

In order to naturally switch the motion states of the remote robot, the position–velocity and position–position hybrid mapping based on automatic switching is designed in this paper, as shown in Fig. 6, so that the position  $\mathbf{P}_m$  and  $\mathbf{Q}_m$  are mapped to  $\boldsymbol{\eta}$  and  $\mathbf{Q}_s$ , respectively. Since the mobile platform is able to move freely with the velocity command, the asymmetrical mapping from the local limited workspace to the remote unlimited workspace is achieved.

To achieve the smooth switch, the switching coefficients are designed as follows:

The states of MM can be decoupled into navigation state and manipulation state, therefore, the coefficients  $\xi_b, \xi_s$  ( $\xi_b = (\xi_v, \xi_\omega)^T, \xi_s = (\xi_\theta, \xi_r, \xi_h)^T$ ) can be used to characterize the motion states of the mobile platform and the manipulator. That is,  $\xi_v = 1$  or  $\xi_\omega = 1$  means that the mobile platform is in motion, while  $\xi_\theta = 0, \xi_r = 0$  or  $\xi_h = 0$  means that the manipulator is stationary, and  $0 < \xi_i < 1, i = v, \omega, \theta, r, h$  means that it is in transition.

It is hoped that the switching coefficients can be related to the closest distance  $d$  between MM and the targets/obstacles, as well as

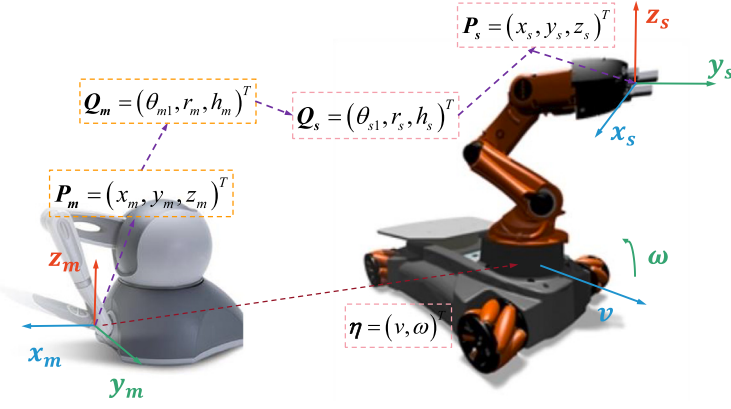
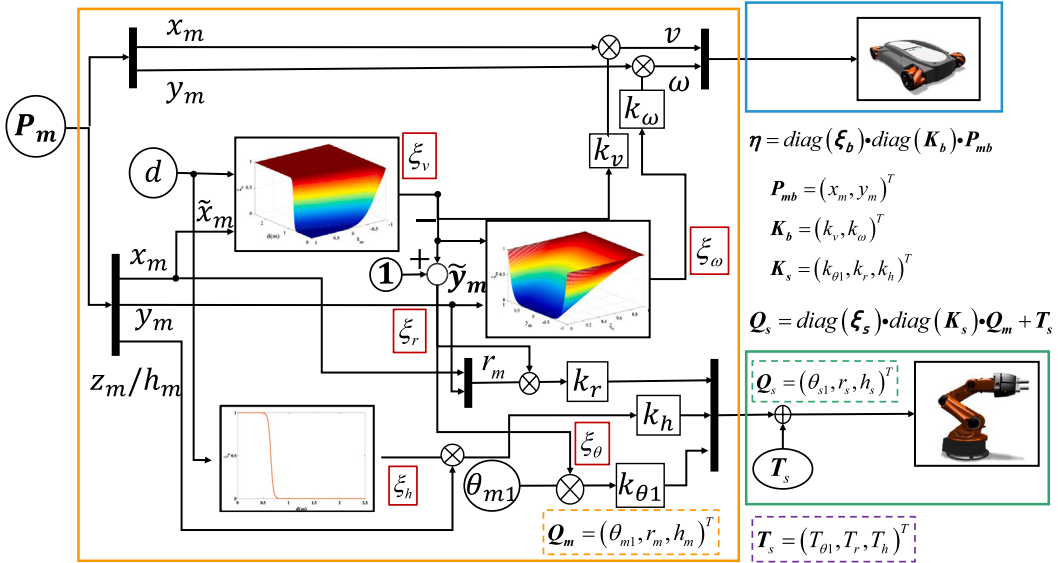


Fig. 5. Asymmetrical mapping of local and remote robot states.



**Fig. 6.** Hybrid asymmetrical mapping based on automatic switching. The local operator generates a position command  $P_m$ , which can be mapped to  $\eta$  to control the movement of the remote mobile platform, or to  $Q_s$  to control the movement of the remote manipulator. Meanwhile, the automatic switching coefficient ( $\xi_i$ , circled with red squares) are designed as the mapping scale factors to switch between these two mapping modes.

the local position command  $P_m$ , as shown in (6).

$$\begin{aligned} \xi_v(d, \tilde{x}_m), \xi_\omega(\tilde{y}_m, \xi_v) \\ \xi_r(d, \tilde{x}_m), \xi_h(\tilde{y}_m, \xi_v), \xi_h(d) \end{aligned} \quad (6)$$

where,  $\tilde{x}_m$  and  $\tilde{y}_m$  are the normalized variables of  $x_m$  and  $y_m$ , respectively, defined as (7):

$$\tilde{x}_m = \frac{x_m}{\max(x_m)}, \tilde{y}_m = \frac{y_m}{\max(y_m)}, \quad (7)$$

so as to satisfy the expression:  $\tilde{x}_m \in [-1, 1], \tilde{y}_m \in [-1, 1]$ .

Therefore, the design principle of the above automatic switching coefficients is shown in Algorithm 1, where the constant  $d_1$  is the safe distance at which the mobile platform will stop, while  $d_2$  is the transition distance at which the navigation state and manipulation state begin to change.

In Algorithm 1, the switching of the motion state of MM is progressive, that is, the switching coefficient  $\xi_i, i = v, \omega, r, \theta, h$  is a continuous function( $\dot{\xi}_i = L_\infty$ ).

Possible forms the functions  $\xi_v, \xi_\omega, \xi_h$  can be seen in Fig. 7, while  $\xi_r, \xi_\theta$  could be simply stated as  $\xi_r = 1 - \xi_v$  and  $\xi_\theta = 1 - \xi_\omega$ .

The specific functional form of  $\xi_i$  depends on practical applications and other implementation tools (neural networks, wave variable

---

#### Algorithm 1 Design of the Automatic Switching Coefficients.

```

Input:  $d, \tilde{x}_m, \tilde{y}_m$ 
Output:  $\xi_v, \xi_\omega, \xi_\theta, \xi_r, \xi_h$ 
1: if  $d > d_2$  then
2:    $\xi_v \approx 1, \xi_\omega \approx 1, \xi_h \approx 0$ 
3: else if  $d_1 < d \leq d_2$  then
4:    $0 < \xi_v < 1, 0 < \xi_\omega < 1, 0 < \xi_h < 1$ 
5: else
6:    $\xi_v \approx 0, \xi_\omega \approx 0, \xi_h \approx 1$ 
7:   if  $|\tilde{y}_m| \rightarrow 1$  then
8:      $\xi_\omega \rightarrow 1$ 
9:   end if
10:  if  $\tilde{x}_m < 0$  and  $\tilde{x}_m \rightarrow -1$  then
11:     $\xi_v \rightarrow 1$ 
12:  end if
13: end if
14:  $\xi_r = 1 - \xi_v, \xi_\theta = 1 - \xi_\omega$ 
15: return  $\xi_v, \xi_\omega, \xi_\theta, \xi_r, \xi_h$ 

```

---

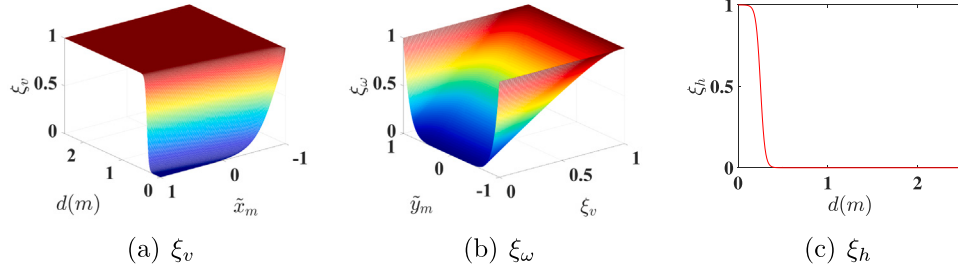


**Fig. 7.** The automatic switching coefficients: (a) shows the variation of  $\xi_v$  with  $d$  and  $\tilde{x}_m$ . When  $d$  is large, that is, MM is far from the target/obstacle,  $\xi_v$  is about 1, so the mobile platform can move freely, otherwise when  $d$  decreases,  $\xi_v$  gradually decreases towards 0, so the mobile platform gradually comes to a stop. However, when  $\tilde{x}_m < 0$  approaches  $-1$ ,  $\xi_v$  gradually increases towards 1, enabling the mobile platform to respond to the command to move backwards. (b) shows the variation of  $\xi_\omega$  with  $\xi_v$  and  $\tilde{y}_m$ . The changes of  $\xi_\omega$  and  $\xi_v$  are basically consistent, but when  $|\tilde{y}_m|$  tends to 1,  $\xi_\omega$  tends to 1, that is, the mobile platform always responds to the rotation command. In (c),  $\xi_h$  is solely determined by  $d$ , where  $\xi_h$  increases from 0 to 1 when  $d$  gets small, indicating that the remote manipulator is allowed to move in the vertical direction only when it approaches the target or obstacle.

control, etc.). In this paper, a basic application of heterogeneous tele-operation for MM is presented as an example to explicitly implement each  $\xi_i$ , which is designed as (8).

$$\begin{cases} \xi_v = 1 - \frac{1}{2} \{\tanh[\alpha(d + \beta)] - \tanh[\alpha(d - \beta)]\} \\ \xi_\omega = 1 - (1 - \xi_v)(1 - \tilde{y}_m^{2n}) \\ \xi_r = 1 - \xi_v \\ \xi_\theta = 1 - \xi_v \\ \xi_h = 1 - \frac{1}{2} \{\tanh[k(d - \lambda)] + 1\}, \end{cases} \quad (8)$$

where  $k, n$  are constant coefficients, and  $\lambda, \alpha, \beta$  satisfy (9).

$$\begin{cases} \lambda = (d_1 + d_2)/2 \\ \beta = \frac{1}{2} [d_2(\tilde{x}_m + 1)] \\ \alpha = 2 \{d_1 [\tanh(8.5\tilde{x}_m + 9) - \beta]\}^{-1} \end{cases} \quad (9)$$

The design of  $\xi_i$  makes it possible to smoothly switch motion states of the remote robot. Then, the specific design of the hybrid asymmetrical mapping is as follows.

Firstly, the position–velocity mapping strategy is used to remotely operate the motion of the mobile platform. So the mapping based on automatic switching is described as (10):

$$\boldsymbol{\eta} = \text{diag}(\xi_b) \cdot \text{diag}(\boldsymbol{K}_b) \cdot \boldsymbol{P}_{mb} \quad (10)$$

where  $\boldsymbol{\eta} = (v, \omega)^T$ ,  $v$  is the linear velocity of the mobile platform, and  $\omega$  is the angular velocity.  $\boldsymbol{K}_b = (k_v, k_\omega)^T$  is the constant scale mapping vector, and  $\boldsymbol{P}_{mb} = (x_m, y_m)^T$  is the position command of the operator.

Besides, in manipulation task, the operator operates the remote manipulator to accomplish pick-up and placement assignments through position–position mapping. Combined with the structural characteristics of the local and remote manipulators, joint-*rh*-profile mapping is adopted, while the coefficients  $\xi_\theta$ ,  $\xi_r$  and  $\xi_h$  are also applied into the mapping to ensure the smooth automatic switching, so that the mapping equation is as (11):

$$\boldsymbol{Q}_s = \text{diag}(\xi_s) \cdot \text{diag}(\boldsymbol{K}_s) \cdot \boldsymbol{Q}_m + \boldsymbol{T}_s \quad (11)$$

where  $\boldsymbol{K}_s = (k_{\theta 1}, k_r, k_h)^T$  is the constant proportion mapping vector that can maximally cover the *rh*-profile of the remote manipulator, and  $\boldsymbol{T}_s = (T_{\theta 1}, T_r, T_h)^T$  is the constant translation vector between the local and remote workspace along the  $r$ -,  $h$ - axes. After mapping, the end boundary contour of the local robot and the reachable area of the *rh*-profile of the remote manipulator are shown in Fig. 8.

**Remark 1.** Through the position–velocity and position–position hybrid asymmetrical mapping algorithm based on automatic switching, the velocity  $\boldsymbol{\eta}$  and the end position  $\boldsymbol{Q}_s$  can be obtained in (10) and (11)

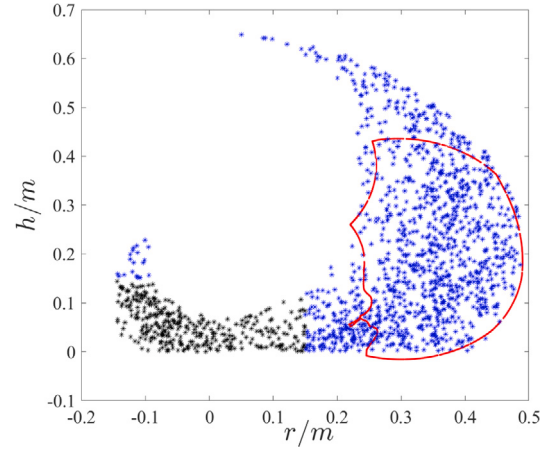


**Fig. 8.** The *rh*-profile of the remote manipulator and the local robot after mapping. The red curve is the mapped end boundary contour of the local robot, while the blue area indicates the reachable region of the end effector of the remote manipulator. The black area is the region where the end effector of the remote manipulator would collide with the mobile platform.

respectively. Subsequently, the automatic switching coefficients  $\xi_b$  and  $\xi_s$ , which are related to the distance  $d$  and the local command  $\tilde{x}_m, \tilde{y}_m$  in (8), can enable smooth switching between the two mapping modes of the remote robot and between different motion states, respectively.

### 3.3. Automatic-switching-based force feedback mapping design

Furthermore, in this system, the force feedback should also be matched with the remote tasks. The overall framework of mapping from the environment to the force feedback is shown in Fig. 9, where  $\boldsymbol{d}_{b,o}$  and  $\boldsymbol{d}_{s,t}$  represent distance information, while  $f_{tou}$  is the measured value of the force sensor fixed on the EE of the remote manipulator. Additionally,  $f_b$  and  $f_s$  correspond to the force feedback during the navigation state and manipulation state, respectively. The combined force feedback  $\boldsymbol{F}_e$  is as (12).

$$\boldsymbol{F}_e = \boldsymbol{F}_b + \boldsymbol{F}_s = \xi_v \boldsymbol{f}_b + \xi_h \boldsymbol{f}_s, \quad (12)$$

where  $\boldsymbol{f}_b$  refers to the virtual guidance force feedback of the mobile platform in the navigation state, which can be generated by the APF method that maps the obstacle constraints to repulsive forces. On the other hand, the force feedback  $\boldsymbol{f}_s$  in the manipulation state can be achieved through automatic switching between the virtual guidance

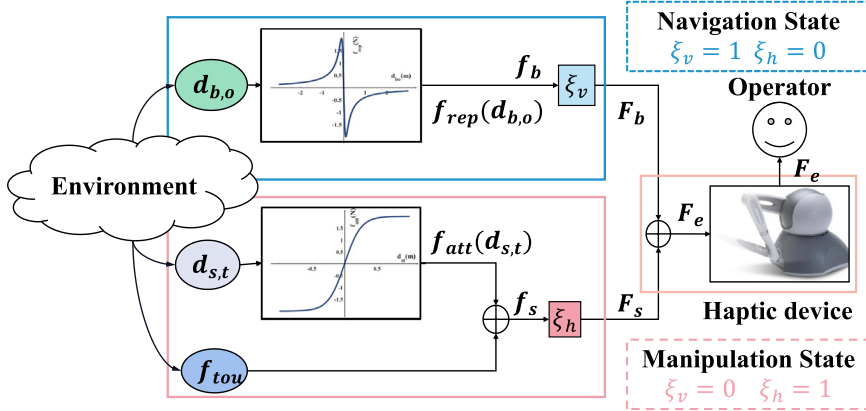


**Fig. 9.** Force feedback mapping framework based on automatic switching. The distance  $d_{b,o}$  is mapped to force  $f_b$  (shown in the blue box) using (14), while the distance  $d_{s,t}$  is mapped to force  $f_s$  (shown in the pink box) through (13) and (15). The automatic switching coefficients  $\xi_v, \xi_h$  as designed above, determine the switching of these different force feedback mapping terms ( $f_b$  and  $f_s$ ), ultimately resulting in the combined force  $F_e$  being fed back to the local side.

force feedback of the remote manipulator and the measured value of the force sensor. Therefore,  $f_b$  and  $f_s$  can be defined as (13).

$$f_b = f_{rep}(d_{b,o}), \quad f_s = f_{att}(d_{s,t}) + f_{tow}, \quad (13)$$

where vectors  $d_{b,o}, d_{s,t}$  respectively represent the distance vector from the mobile platform to the obstacle and the distance vector from the EE of the remote manipulator to the target.  $f_{rep}$  is the repulsive force feedback mapped by the obstacle constraint,  $f_{att}$  is the attractive force mapped by the target constraint, and  $f_{tow}$  is the measured value of the force sensor, which can be respectively written as (14) and (15).

$$f_{rep}(d_{b,o}) = \frac{-k_{b1}d_{b,o}}{k_{b1}\|d_{b,o}\|_2^2 + 1}, \quad k_{b1}, k_{b2} \in \mathbb{R}^+ \quad (14)$$

$$f_{att}(d_{s,t}) = k_{s1} \tanh(k_{s2}d_{s,t}), \quad k_{s1}, k_{s2} \in \mathbb{R}^+ \quad (15)$$

Therefore,  $f_{rep}$  and  $f_{att}$  have the following properties:

- As  $d_{b,o}$  decreases monotonically to 0,  $f_{rep}$  increases monotonically to a certain boundary value, and its direction does not change suddenly. When the mobile platform is far away from the obstacle,  $f_{rep}$  remains about 0.
- $f_{att}$  could monotonically decrease to 0 as  $d_{s,t}$  decreases. When  $f_{att}$  reaches 0, it indicates that the EE has grasped the target object. At this point, the force measured by the force sensor should be fed back to the operator, enabling the automatic switching between these two types of forces in the manipulation state.

The curves of  $f_{rep}(d_{b,o})$  and  $f_{att}(d_{s,t})$  in one direction are shown in Fig. 10.

**Remark 2.** Based on the switching coefficients  $(\xi_v, \xi_h)$ , the force feedback  $F_e$  designed as (12) can automatically and smoothly switch the force between the remote mobile platform and the manipulator, as well as the virtual guiding force and the operation force measured by the force sensor mounted on the manipulator. Therefore, the force feedback can be matched with the remote tasks and accomplish the automatic switching during the teleoperation of the MM.

#### 4. Semi-physical simulation experiment

In this section, to demonstrate the effectiveness and superiority of the proposed framework in practical teleoperation systems, the comparative semi-physical simulations are carried out, since the performance

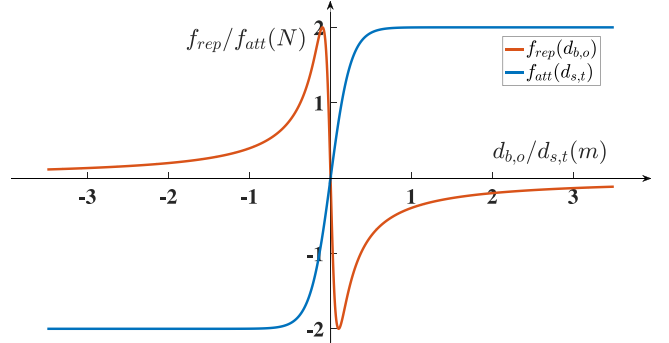


**Fig. 10.**  $f_{rep}(d_{b,o})$  and  $f_{att}(d_{s,t})$  in one direction.

of the system will be influenced by various factors such as the technology employed for its implementation (e.g., actual robotic platform, channel delay, vision or force feedback).

#### 4.1. Simulation setup

As shown in Fig. 5, the haptic device Phantom Omni, equipped with two freely programmable buttons, is employed as the local device with kinematics (1), which has 6 DOFs positional sensing and 3 DOFs force feedback to make the operator feel the virtual object, and its controller is implemented on Matlab-Simulink using the PHAN-SIM TOOLKIT Library. Meanwhile, the remote robot are simulated in the CoppeliaSim robotic simulator with kinematics (2)–(5). And the Hokuyo Urg04, a laser radar installed on the front of the MM, is used to detect and measure the real-time distance to the targets/obstacles in the environment.

To verify the improvement of the proposed framework on teleoperation efficiency and friendliness, a navigate-manipulate-navigate-manipulate task with visual and force feedback is designed. More specifically, the task requires the operator to use the local haptic device to control the remote mobile manipulator to perform sequential actions. The first action is to depart from an initial location and move to a target work area (navigation). Then, the operator needs to pick up an object (manipulate) and travel to another target location (navigation) to place the object (manipulate). Throughout the task, the operator can sense

**Table 2**  
Selection of parameters in S2.

Parameters	Value
$K_b$	$(1.5, 1)^T$
$K_s$	$(\frac{\theta_{m1\max} - \theta_{m1\min}}{\theta_{s1\max} - \theta_{s1\min}}, 1.6, 1.5)^T$
$T_s$	$\left( \left( 1 - \frac{\theta_{m1\max} - \theta_{m1\min}}{\theta_{s1\max} - \theta_{s1\min}} \right) \theta_{m1\min}, 0.1, 0.2 \right)^T$

the remote visual and force feedback, thereby effectively operating the remote robot to complete tasks.

In the simulation, the distance range between the remote robot and the obstacle/target is set to  $d \in [0, 5]$  m. The safe distance and transition distance in (9) are respectively set as  $d_1 = 0.15$  m and  $d_2 = 0.35$  m.

To ensure a fair comparison, two switchers are compared to implement the same navigate-manipulate-navigate-manipulate task.

S1: The traditional manual-button-based switching framework with constant scale position mapping and without force feedback [17].

S2: The novel continuous-automatic-based switching framework with asymmetrical mapping and force feedback proposed in this paper, where the mapping relationship and force feedback are selected as (10)–(11) and (12)–(15), and the boundary of force feedback is set as  $3.5N$ . Wherein, after experimental testing, the selection of these parameters is shown in Table 2.

#### 4.2. Simulation results

Figs. 11 and 12 show the comparative results of the switching coefficients in S1 and S2, respectively, and the mapping signals (10) and (11) are also shown. Due to the fact that the remote robot is switched manually by pressing a button in S1 during its motion, the button-based switching is not smooth enough, which would make the mapping reference change steeply and result in an unstable state. Furthermore, the manual switching impels the operator to constantly monitor the motion state of the remote robot in preparation for each switch. As a result, it will take more time and place additional mental burden on the operator when performing the same task. However, the whole switching and mapping tasks of S2 evolve continuously and stably, which allow the operator to automatically switch the motion state of the remote robot without being distracted by being prepared to switch. Consequently, the task can be more straightforward to complete with S2, which is reflected in shorter time to complete the same task.

Meanwhile, the force feedback  $F_e$ ,  $F_s$  and  $F_b$  are also recorded as shown in Fig. 13, where the red curve represents the force feedback of the mobile platform ( $F_b = \xi_v f_b$ ). In the navigation state, when the mobile platform approaches an obstacle,  $F_b$  increases significantly, so the operator could mainly feel the repulsion force feedback from the obstacle, while in the manipulation state,  $F_b$  smoothly transitions to a value close to 0. The blue curve represents the force feedback of the remote manipulator ( $F_s = \xi_h f_s$ ). When the MM is in the navigation state,  $F_s$  basically remains at 0. However, during the transition to the manipulation state,  $F_s$  begins to change smoothly, allowing the operator to primarily sense the attraction force feedback from the target. When the EE successfully grasps the target object, the attraction force automatically switches to the contact force between the EE and the target object, which is measured by the force sensor. The black curve indicates the resultant force  $F_e$ , which can switch automatically and smoothly between  $F_b$  and  $F_s$ . The above force feedback results show that in this task, the force that is fed back to the operator can match with the remote tasks and realize the smooth and automatic switching between the force feedback of the mobile platform and the manipulator. Therefore, compared to relying solely on visual feedback, the operator could better sense the remote unstructured environment with the assistance of force feedback.

**Table 3**  
Averaged results.

	Manual switching (S1)		Automatic switching (S2)	
Remote Robot	$T_{task}(s)$	$P_o(\text{Workload})$	$T_{task}(s)$	$P_o(\text{Workload})$
Simulation Robot	82.5	80.7	64.4	60.2
Real Robot	75.6	83.3	56.3	62.5

To make a preliminary quantitative comparison between these two frameworks, 3 different operators repeat the tests for each switching framework 5 times. Due to the fact that in actual teleoperation scenarios, the task completion time and operator's workload are better indicators of the quality of the operating method, where the workload was quantified using NASA Task Load Index (NASA-TLX), as detailed in the experimental section. Therefore, the data obtained are averaged and presented in Table 3. It can be seen that whether the remote robot is simulated or real, S2 can effectively reduce the task completion time( $T_{task}(s)$ ), and the workload ( $P_o$ ) is also smaller compared to S1 (where a larger  $P_o$  indicates a higher operator's workload). This indicates that S2 outperforms S1, demonstrating its superior performance.

## 5. Physical experiment

### 5.1. Experiment setup

To evaluate the performance of the teleoperation system based on automatic switching under real conditions, the same experiment of S2 was also carried out on a real mobile robot. Specifically, the navigate-manipulate-navigate-manipulate teleoperation task was executed on a real mobile manipulator using the framework proposed in this paper. It is implemented on the Robot Operating System (ROS) as shown in Fig. 14.

To further evaluate whether the proposed teleoperation framework is more user-friendly and intuitive for operators, 5 volunteers (aged 20–26, 3 men and 2 women, with normal or corrected normal vision, without physical disabilities, and without the foundation of robot knowledge) were invited to carry out the user study. Before the experiment, all participants were instructed to do a learning and training session, i.e., using the actual haptic device Phantom Omni to operate the real KUKA-Youbot to complete the task of navigating and manipulating, and then the participants practiced until they felt confident to start the experimental trial. Afterward, they were required to perform 15 identical assignments for each group of experiments, and the average value of these 15 assignments was taken as the experimental result. Additionally, it is important to note that in order to prevent operators from becoming accustomed to a specific mode, the test sequence and methods were randomly carried out.

During the experiment, in order to evaluate the improvement in user-friendliness of each unit in the framework based on automatic switching, 5 comparative cases were set as follows.

- C1: Manual switching; no asymmetric mapping; no force feedback;
- C2: Automatic switching; asymmetric mapping; no force feedback;
- C3: Manual switching; asymmetric mapping; force feedback;
- C4: Automatic switching; no asymmetric mapping; force feedback;
- C5: Automatic switching; asymmetric mapping; force feedback;

Furthermore, in order to evaluate the workload of the different cases from multiple dimensions, the NASA Task Load Index (NASA-TLX) [36] was utilized in this paper. Namely, the evaluations are conducted on six scales: Mental Demand ( $I_1$ ), Physical Demand ( $I_2$ ), Temporal Demand ( $I_3$ ), Performance ( $I_4$ ), Effort ( $I_5$ ) and Frustration ( $I_6$ ). The volunteers were instructed to rate each scale after completing each experiment. Each scale was divided into 20 equal intervals, ranging from 0 as the initial value to 100 as the maximum value, with an increment of 5 between each interval, which aimed to determine the magnitude of the

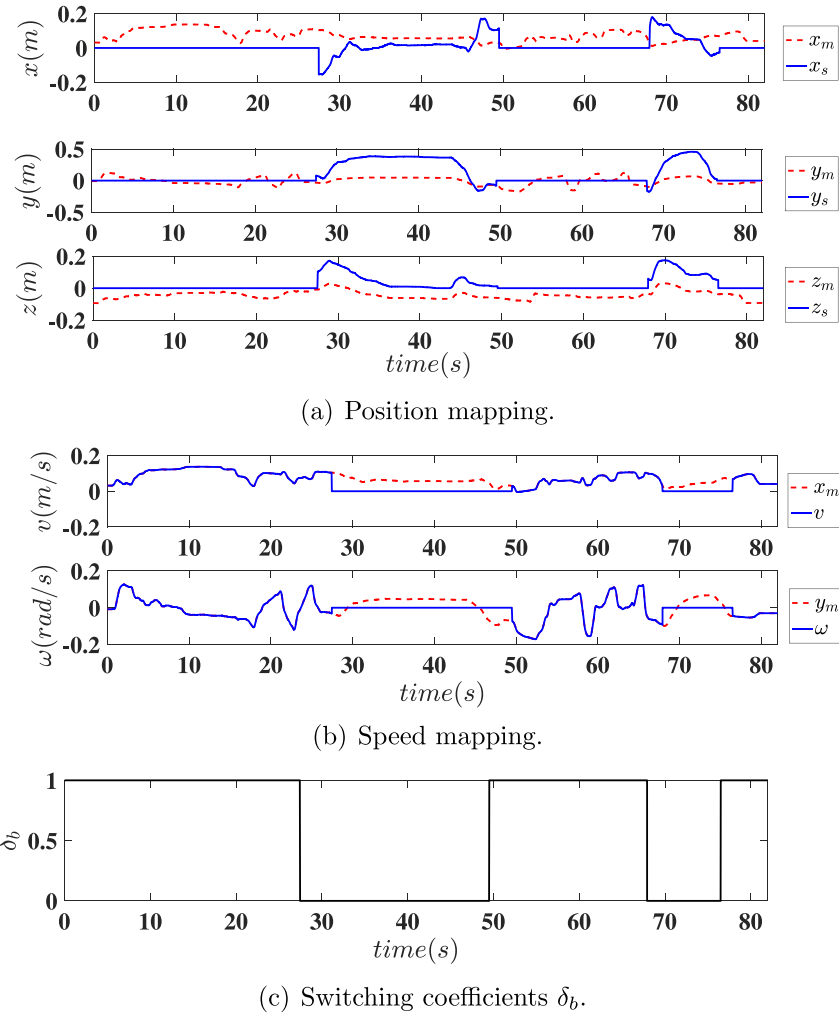


**Fig. 11.** Evolution of the mapping signal and switching coefficients for S1.

factor's impact on a specific task. Therefore, the indicator  $P_o$  is designed to quantify the workload as (16):

$$P_o = \frac{1}{n} \sum_{i=1}^n I_i, n = 6 \quad (16)$$

## 5.2. Experiment results and user study analysis

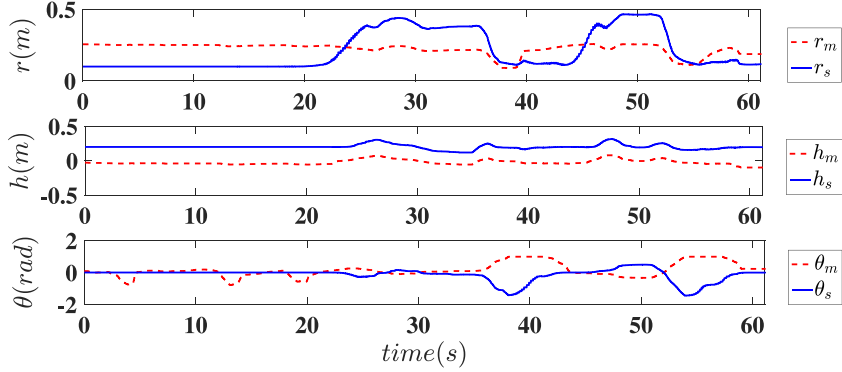
The entire automatic switching process of S2 on a real mobile robot can be observed in Fig. 15. Similarly, 3 operators repeated the tests for each switching framework (S1 and S2) 5 times. The data is also averaged and recorded in Table 2. It can be seen that S2 can effectively reduce the task time by approximately 25% and alleviate the operator's workload compared to S1 under real conditions.

The statistical results (six scales  $I_i, i = 1, 2, 3, 4, 5, 6$  of the NASA-TLX rated by the volunteers) of the user study were plotted using the boxplot toolbox in Matlab as shown in Fig. 16. Since C1 only has manual switching and does not consider the asymmetric mapping and force feedback, its workload index  $P_o$  is the highest. However, C2, C3, C4 and C5 have significantly reduced their workload because of the automatic switching, asymmetric mapping and force feedback algorithms proposed in this paper. Among them, automatic switching and asymmetric mapping are adopted in C2, resulting in the most significant reduction in workload compared to C1. Therefore, it can be

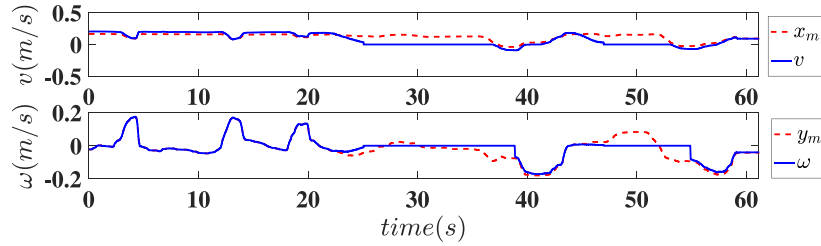
concluded that the switching and mapping modes have a more direct impact on the operator's remote operation.

Furthermore, Fig. 16 also provides the individual survey results for obtaining the workload index  $P_o$ . Since there is no asymmetric mapping in C4, the  $I_2$  of the operator is increased by 29% compared to that in C5. This is attributed to the fact that the remote KUKA-Youbot has a larger workspace compared to the haptic device Phantom Omni. As a result, the operator needs to operate the local device in a larger range, thus increasing the physical demand of the operator. Since the manual switching is adopted in C3, the workload of the operator is increased by 19% compared to C5. This is because the manual switching requires the operator to constantly monitor the motion state of the remote robot and timely switch the motion state by pressing a button. In addition, the mobile platform needs to be constantly adjusted to a suitable position through the button before performing the manipulation task, which significantly increases the physical and mental demands on the operator.  $I_5$  of C5 is approximately 28% lower than that of C2, mainly because the force feedback can guide and assist the operator to sense the remote environment. And the absence of the force perception in C2 requires the operator to operate the manipulator more carefully to avoid the collision with obstacles.

The volunteers expressed that in all cases, the automatic-based framework is more user-friendly and straightforward for the operator, which is reflected in shorter task completion time and reduced workload. In conclusion, the framework proposed in this paper has better



(a) Position mapping.



(b) Speed mapping.

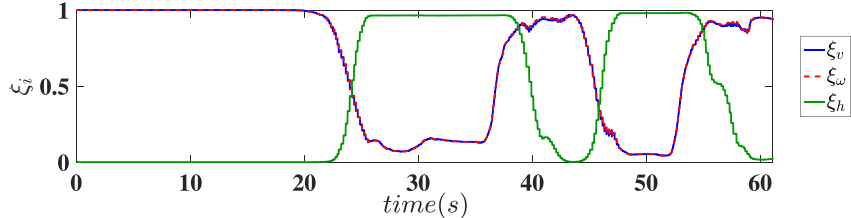
(c) Switching coefficients  $\xi_i$ .

Fig. 12. Evolution of the mapping signal and switching coefficients for S2.

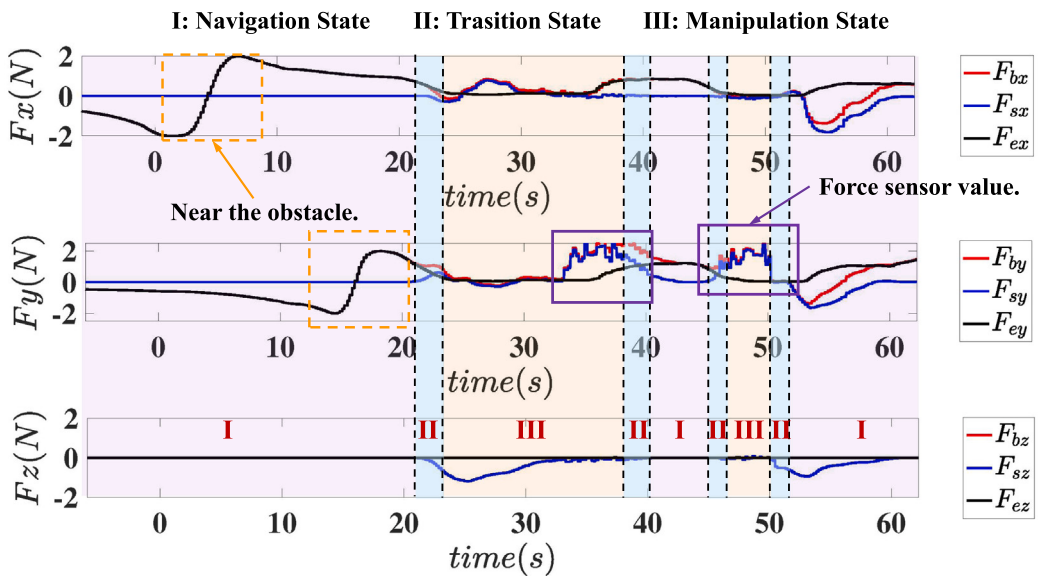
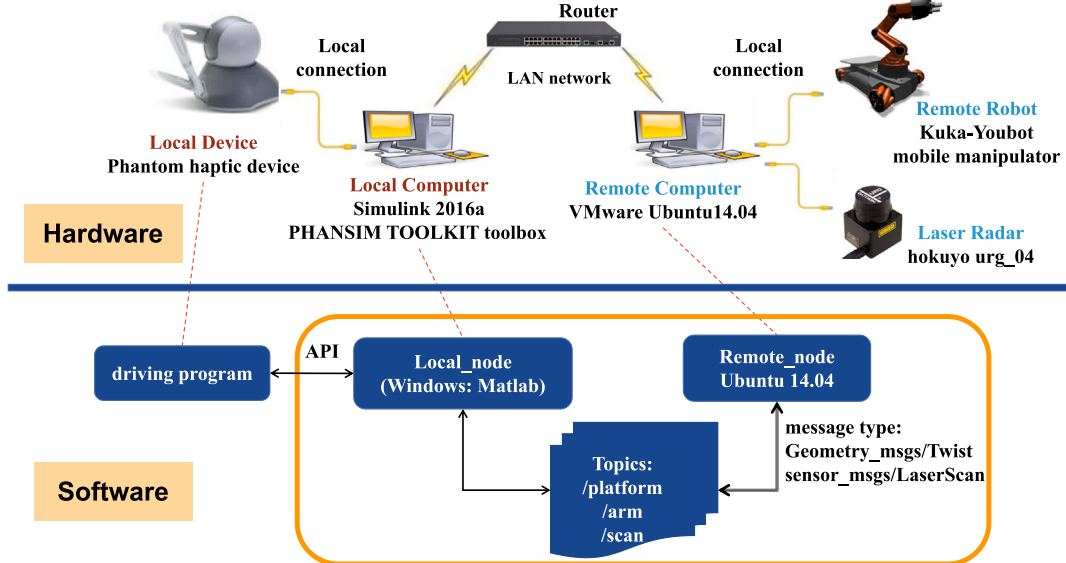
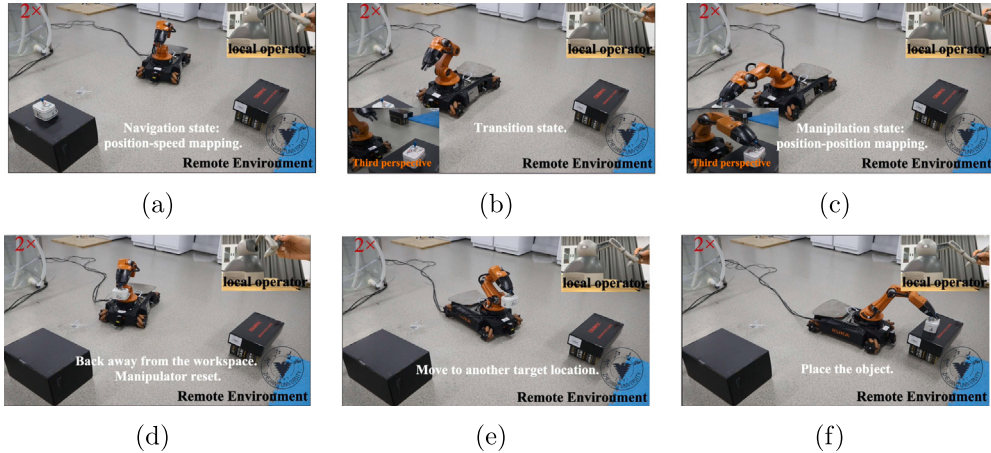


Fig. 13. The force feedback evolution of S2.



**Fig. 14.** The experimental software and hardware systems. The local haptic device Phantom Omni runs within the Matlab/Simulink software of the Windows system, while the remote KUKA-Youbot runs on the Robot Operating System (ROS). The local and remote sides are connected via a LAN network and communicate through ROS topics. The laser radar is installed in front of the mobile robot to detect real-time distance to targets/obstacles, and then transmits the distance information to the local side.



**Fig. 15.** The automatic switching process of the teleoperated mobile manipulator: (a) Navigation state: move to the target area; (b) Navigation transition to manipulation state; (c) Manipulation state: pick up the target object; (d) Navigation state: back away from the target area; (e) Navigation state: move to another location; (f) Manipulation state: place the target object.

performance compared to the manual-based framework, since it can reduce the decision-making pressure on the operator and improve the security of the teleoperation system.

## 6. Conclusions

To address the problem of heavy operator workload caused by heterogeneous teleoperation, an automatic-switching-based teleoperation framework for MM is developed in this paper. In particular, to ensure the infinite remote workspace being covered with the limited local workspace, the continuously varying coefficients  $\xi_i$  are proposed,

based on which the motion states of the remote robot can be automatically switched between position–velocity and position–position modes. Meanwhile, the automatic-switching-based force feedback is further designed and matched with the remote tasks, making that the operator senses the remote unstructured environment better. Comparative experiments are carried out with a user study, where the results show that less time is needed to complete tasks and the decision-making pressure of operator decreases, demonstrating that this novel framework is more intuitive and user-friendly for the operator. Therefore, the teleoperation framework proposed in this paper will be helpful to improve the security and efficiency in remote tasks of practical applications.

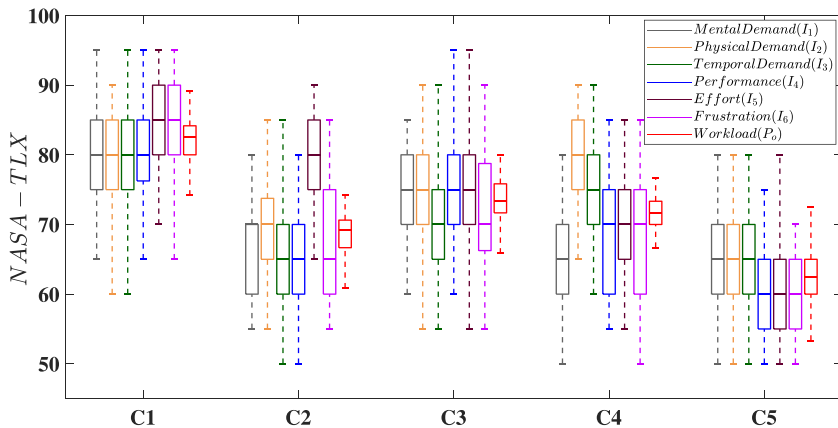


**Fig. 16.** The user study results of NASA-TLX. The statistical results of C5 in these six scales and  $P_o$  are superior or not inferior to C1-C4, as it is a teleoperation framework composed of automatic switching, asymmetric mapping, and force feedback.

In future work, to further extend the potential applying scenarios of the proposed method, other modalities such as speech and voice will be studied to control the movement of remote robot.

#### CRediT authorship contribution statement

**Wenwen Li:** Conceptualization, Methodology, Data processing, Formal analysis, Investigation, Writing – original draft, Writing – review & editing. **Fanghao Huang:** Formal analysis, Investigation, Conceptualization, Methodology, Writing – review & editing, Supervision. **Zihao Chen:** Data processing, Validation, Writing – review & editing. **Zheng Chen:** Conceptualization, Methodology, Funding acquisition, Resources, Supervision.

#### Declaration of competing interest

The authors declare that they have no known competing financial interests or personal relationships that could have appeared to influence the work reported in this paper.

#### Data availability

Data will be made available on request.

#### References

- [1] Xing H, Gong Z, Ding L, Torabi A, Chen J, Gao H, et al. An adaptive multi-objective motion distribution framework for wheeled mobile manipulators via null-space exploration. *Mechatronics* 2023;90:102949.
- [2] Ding L, Xing H, Torabi A, Mehr JK, Sharifi M, Gao H, et al. Intelligent assistance for older adults via an admittance-controlled wheeled mobile manipulator with task-dependent end-effectors. *Mechatronics* 2022;85:102821.
- [3] Sun W, Yuan Y. Passivity based hierarchical multi-task tracking control for redundant manipulators with uncertainties. *Automatica* 2023;155:111159.
- [4] Liao J, Chen Z, Yao B. Model-based coordinated control of four-wheel independently driven skid steer mobile robot with wheel-ground interaction and wheel dynamics. *IEEE Trans Ind Inf* 2019;15(3):1742–52.
- [5] Liu Y, Li Z, Su H, Su CY. Whole-body control of an autonomous mobile manipulator using series elastic actuators. *IEEE/ASME Trans Mechatronics* 2021;26(2):657–67.
- [6] Yoon WK, Goshozono T, Kawabe H, Kinami M, Tsumaki Y, Uchiyama M, et al. Model-based space robot teleoperation of ETS-VII manipulator. *IEEE Trans Robot Autom* 2004;20(3):602–12.
- [7] Cárdenas EF, Dutra MS. An augmented reality application to assist teleoperation of underwater manipulators. *IEEE Latin Am Trans* 2016;14(2):863–9.
- [8] Chen Z, Zhou S, Shen C, Lyu L, Zhang J, Yao B. Observer-based adaptive robust precision motion control of a multi-joint hydraulic manipulator. *IEEE-CAA J. Automatica Sin* 2024;11(JAS-2023-1081):1.
- [9] Groves K, Hernandez E, West A, Wright T, Lennox B. Robotic exploration of an unknown nuclear environment using radiation informed autonomous navigation. *Robotics* 2021;10(2).
- [10] Smith R, Cucco E, Fairbairn C. Robotic development for the nuclear environment: Challenges and strategy. *Robotics* 2020;9(4).
- [11] Chen Z, Huang F, Sun W, Gu J, Yao B. RBF-neural-network-based adaptive robust control for nonlinear bilateral teleoperation manipulators with uncertainty and time delay. *IEEE/ASME Trans Mechatronics* 2020;25(2):906–18.
- [12] Wang S, Ramos J. Dynamic locomotion teleoperation of a reduced model of a wheeled humanoid robot using a whole-body human-machine interface. *IEEE Robot Autom Lett* 2022;7(2):1872–9.
- [13] Huang F, Chen X, Chen Z, Pan YJ. A novel SMMS teleoperation control framework for multiple mobile agents with obstacles avoidance by leader selection. *IEEE Trans Syst Man Cybern Syst* 2023;53(3):1517–29.
- [14] Zakerimanesh A, Hashemzadeh F, Torabi A, Tavakoli M. A cooperative paradigm for task-space control of multilateral nonlinear teleoperation with bounded inputs and time-varying delays. *Mechatronics* 2019;62:102255.
- [15] Wang S, Ramos J. Dynamic locomotion teleoperation of a reduced model of a wheeled humanoid robot using a whole-body human-machine interface. *IEEE Robot Autom Lett* 2022;7(2):1872–9.
- [16] Yang C, Luo J, Liu C, Li M, Dai SL. Haptics electromyography perception and learning enhanced intelligence for teleoperated robot. *IEEE Trans Autom Sci Eng* 2019;16(4):1512–21.
- [17] Sun D, Liao Q. Asymmetric bilateral telerobotic system with shared autonomy control. *IEEE Trans Control Syst Technol* 2021;29(5):1863–76.
- [18] Andaluz VH, Salinas L, Roberti F, Toibero JM, Carelli R. Switching control signal for bilateral tele-operation of a mobile manipulator. In: 2011 9th IEEE international conference on control and automation. 2011, p. 778–83.
- [19] Santiago DD, Slawinski E, Mut V. Human-inspired stable bilateral teleoperation of mobile manipulators. *ISA Trans* 2019;95:392–404.
- [20] Wrock MR, Nokley SB. Decoupled teleoperation of a holonomic mobile-manipulator system using automatic switching. In: 2011 24th Canadian conference on electrical and computer engineering. 2011, p. 001164–8.
- [21] Santiago D, Slawinski E, Mut VA. Stable delayed bilateral teleoperation of mobile manipulators. *Asian J Control* 2017;19:1140–52.
- [22] Pham CD, From PJ. Control allocation for mobile manipulators with on-board cameras. In: 2013 IEEE/RSJ international conference on intelligent robots and systems. 2013, p. 5002–8.
- [23] Wrock MR, Nokley SB. An automatic switching approach to teleoperation of mobile-manipulator systems using virtual fixtures. *Robotica* 2017;35(8):1773–92.
- [24] Meeker C, Haas-Heger M, Ciocarlie M. A continuous teleoperation subspace with empirical and algorithmic mapping algorithms for nonanthropomorphic hands. *IEEE Trans Autom Sci Eng* 2022;19(1):373–86.
- [25] Mokogwu CN, Hashtrudi-Zaad K. A hybrid position-Crate teleoperation system. *Robot Auton Syst* 2021;141:103781.
- [26] Parkhatdinov I, Ryu JH. Hybrid position-position and position-speed command strategy for the bilateral teleoperation of a mobile robot. In: 2007 international conference on control, automation and systems. 2007, p. 2442–7.
- [27] Pepe A, Chiaravalli D, Melchiorri C. A hybrid teleoperation control scheme for a single-arm mobile manipulator with omnidirectional wheels. In: 2016 IEEE/RSJ international conference on intelligent robots and systems. 2016, p. 1450–5.
- [28] Chen Z, Huang F, Chen W, Zhang J, Sun W, Chen J, Gu J, Zhu S. RBFNN-based adaptive sliding mode control design for delayed nonlinear multilateral telerobotic system with cooperative manipulation. *IEEE Trans Ind Inf* 2020;16(2):1236–47.

- [29] Abdi E, Kulic D, Croft E. Haptics in teleoperated medical interventions: Force measurement, haptic interfaces and their influence on user's performance. *IEEE Trans Biomed Eng* 2020;67(12):3438–51.
- [30] Du G, Han R, Yao G, Ng WWY, Li D. A gesture- and speech-guided robot teleoperation method based on mobile interaction with unrestricted force feedback. *IEEE/ASME Trans Mechatronics* 2022;27(1):360–71.
- [31] Masaki R, Motoi N. Remote control method with force assist based on time to collision for mobile robot. *IEEE Open J Ind Electron Soc* 2020;1:157–65.
- [32] Sławiński E, Santiago D, Mut V. Dual coordination for bilateral teleoperation of a mobile robot with time varying delay. *IEEE Latin Am Trans* 2020;18(10):1777–84.
- [33] Motoi N, Kimura H, Kobayashi M. Experimental operability evaluation of remote control with force feedback for mobile robot. In: 2018 IEEE international conference on industrial technology. 2018, p. 159–64.
- [34] Guajardo-Benavides EJ, Arteaga MA. On the finite time force estimation for bilateral teleoperation of robot manipulators with time varying delays. *Control Eng Pract* 2023;138:105622.
- [35] Liao J, Huang F, Chen Z, Yao B. Optimization-based motion planning of mobile manipulator with high degree of kinematic redundancy. *Int J Intell Robot Appl* 2019;1–16.
- [36] Bischoff R, Huggenberger U, Prassler E. KUKA youBot - a mobile manipulator for research and education. In: 2011 IEEE international conference on robotics and automation. 2011, p. 1–4.



**Wenwen Li** received the B.Eng. degree in ocean engineering and technology from Zhejiang University, Zhejiang, China, in 2022. She is currently working toward the Ph.D. degree in ocean technology and engineering with the Ocean College, Zhejiang University (Zhoushan Campus), Zhoushan, Zhejiang, China. Her research interests mainly focus on the control and planning of robotics and teleoperation systems.



**Fanghao Huang** received the B.Eng. degree in mechanical engineering from Nanchang University, Nanchang, Jiangxi, China, in 2017, and the Ph.D. degree in mechanical engineering from Zhejiang University, Hangzhou, Zhejiang, China, in 2022. Since 2022, he has been a Postdoctoral Researcher with the Ocean College, Zhejiang University (Zhoushan Campus), Zhoushan, Zhejiang, China. His research interests mainly focus on the advanced control of tele-robotic and mechatronic system (e.g., motion control, hybrid motion/force control, visual servoing control).



**Zihao Chen** is currently working toward the B.Eng. Degree in ocean engineering and technology with the Ocean College, Zhejiang University (Zhoushan Campus), Zhoushan, Zhejiang, China. His research interests mainly focus on the control of robotics.



**Zheng Chen** received the B.Eng. and Ph.D. degrees in mechatronic control engineering from Zhejiang University, Zhejiang, China, in 2007 and 2012, respectively. From 2013 to 2015, he was a Postdoctoral Researcher with the Department of Mechanical Engineering, Dalhousie University, Halifax, NS, Canada. Since 2015, he has been with the Ocean College, Zhejiang University (Zhoushan Campus), Zhoushan, China, where he was promoted to the rank of Professor in 2020. His research interests mainly focus on advanced control of robotic and mechatronic system (e.g., nonlinear adaptive robust control, motion control, trajectory planning, tele-robotics, hydraulic system, precision mechatronic system, soft actuator and robot, mobile manipulator, underwater robot, and exoskeleton).